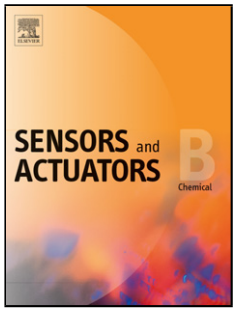

Title: Efficient temperature sensing using photoluminescence of Er/Yb implanted GaN thin films

Authors: N. Hamza, A. Toncelli, Abdul K. Parchur, E. Alves, R. Maalej

PII: S0925-4005(17)30642-1
DOI: http://dx.doi.org/doi:10.1016/j.snb.2017.04.042
Reference: SNB 22128

To appear in: *Sensors and Actuators B*

Received date: 6-2-2017
Revised date: 5-4-2017
Accepted date: 8-4-2017

Please cite this article as: N.Hamza, A.Toncelli, Abdul K.Parchur, E.Alves, R.Maalej, Efficient temperature sensing using photoluminescence of Er/Yb implanted GaN thin films, Sensors and Actuators B: Chemicalhttp://dx.doi.org/10.1016/j.snb.2017.04.042

Efficient temperature sensing using photoluminescence of Er/Yb implanted GaN thin films

N. Hamza[a],A. Toncelli[b], Abdul K. Parchur[d]*, E. Alves[c] ,R. Maalej[a]*

[a]Laboratoire Géoressources, Matériaux, Environnement et Changements Globaux, Faculty of Sciences of Sfax, UniversityofSfax, 3018 Sfax, Tunisia

[b]NEST-IstitutoNanoscienze CNR, PhysicsDepartment "Enrico Fermi", University of Pisa, Largo B. Pontecorvo, 3, 56127 Pisa, Italy

[c]IPFN, Instituto Superior Tecnico, Universidade de Lisboa, EstradaNacional 10, 2695-066 Bobadela LRS, Portugal

[d]Department of Physics,BanarasHinduUniversity, Varanasi, 221005 India ;CurrentAddress: Department of Radiology, MedicalCollege of Wisconsin, Milwaukee, WI 53226 USA

*Corresponding author's: ramzi.maalej@fss.rnu.tn andaparchur@mcw.edu

Highlights

- The luminescence characteristics of GaN films implanted with Erbium at low doses were evaluated.
- The temperature dependence of the YL band allowed us to identify the nitrogen-vacancy as the main responsible defect for this emission.
- The color coordinates analysis indicates that Er^{3+}/Yb^{3+} co-doped GaN semiconductor emits at room temperature a blended light with color in the white-light region.
- The significant temperature sensitivity obtained indicates its potential as optical temperature sensing probe in the temperature range 200–300K.
- The maximum sensitivity reached was $15x10^{-4}$ K^{-1} at 200 K.

Abstract

The luminescence characteristics of GaN films implanted with Er at low doses were evaluated. The defect-related yellow luminescence (YL) and green luminescence (GL) bands observed under direct excitation with 488 nm were attributed to the transitions via different charge levels of the same defect. The quenching behavior of the luminescence intensity either with the temperature or concentration variation can be attributed to nonradiative energy transfer (ET)

and/or charge transfer by trapping impurities. The temperature dependence of the YL band allowed us to identify the defect responsible for this emission. The best candidate for this defect was found to be a nitrogen-vacancy. A GaN sample co-doped with Er^{3+} and Yb^{3+} ions was prepared, and its optical properties were analyzed. The incorporation of Yb^{3+} improved the PL emission intensity in the visible region. This feature results from the efficient ET processes between these two doping ions. The color coordinate analysis indicates that Er^{3+}/Yb^{3+} co-doped GaN semiconductor emits light with color in the white-light region. To investigate the temperature sensing application of the synthesized co-doped semiconductor, the temperature-sensing performance was evaluated using the fluorescence intensity ratio technique in the temperature range 200–300K. The significant temperature sensitivity indicates its potential as a temperature sensing probe. The maximum sensitivity was 15×10^{-4} K^{-1} at 200 K.

Keywords: GaN, Er^{3+}, Yb^{3+}, optical spectroscopy, temperature sensing.

1. Introduction

Over the past few decades, photoluminescence (PL) in rare-earth ion (RE)-doped materials have received much attention, particularly because of their potential applications in optoelectronics such as light-emitting diodes, displays, lasers [1–3], and temperature sensors [4]. The luminescent temperature sensor applications using RE^{3+} ions draw great interest of researchers. In fact, temperature can affect the populations of these energy levels according to the Boltzmann distribution law. Thus, a change in temperature influences the emission intensities of these ions. Up to now, various approaches have been expanded to achieve a high detection sensitivity; the fluorescence intensity ratio (FIR) technique being the most used one [5]. In particular, the FIR technique uses the temperature-dependent PL emission intensity arising from two close thermally coupled levels of RE^{3+} ions.

Among the RE ions, the trivalent Er ion (Er^{3+}) shows a wide and complex emission spectrum ranging from UV to mid-IR regions [7]. The intensity of these fluorescence lines depends on the probability of a particular transition, which in turn is a function of the ligand field of the surrounding environment. Er^{3+} ion presents an elaborate energy state scheme with different energy gaps, its energy levels are distributed within the energy space, and the lifetimes of some levels are long enough to make Er^{3+} interesting

as an upconverting luminescent center. The sensitization of Er-doped host–lattice with Yb^{3+} ions is a popular method for increasing the optical pumping efficiency owing to the high absorption cross-section of Yb ions leading to an efficient Yb^{3+}–Er^{3+} energy transfer (ET) [6].

As an activator, trivalent Er ion has attracted particular interest because of its several efficient emission bands [8–10]: The 1.55-μm spectral band (IR emission) belonging to the $^4I_{13/2} \rightarrow {}^4I_{15/2}$ transition is considered ‘‘eye-safe” and has already been used to develop lasers for medicine, telemetry, telecommunication, and remote sensing [11]. The green emission or 550-nm emission band corresponding to the $(^2H_{11/2}, {}^4S_{3/2}) \rightarrow {}^4I_{15/2}$ transitions is important in developing compact laser devices for display and data storage applications.

In fact, thanks to the advance witnessed in semiconductor photonic device techniques and design, many researchers have dedicated their efforts to introduce Er^{3+} ions into semiconductors, resulting in photonic integrated circuits with multiple functionalities [12, 13]. Among the different combinations of RE ions and nitrides hosts, GaN:Er is one of the most interesting combination. In fact, Er-doped GaN has many potential applications in optoelectronics [14, 15], and it is one of the most efficient host matrix for providing high emission quantum yields at room temperature in the IR and visible spectral ranges [16], because the thermal stability of Er emission in GaN host lattice is the highest compared to small-band-gap semiconductor materials [17]. Moreover, GaN can be doped with RE^{3+} ions at high concentrations with perfect uniformity.

Therefore, GaN has the advantages suitable for integrated photonic applications. Compared to other semiconductors such as GaAs or Si [18], GaN crystals often exhibit a superior optical performance. Moreover, it is of great interest because of its exceptional properties including a direct-band-gap transition, which has an important role in optical applications, a large energy band gap (3.4 eV at room temperature) results in a very high thermal stability and mechanical robustness.

Among the various methods used in the growth of GaN thin films, molecular beam epitaxy (MBE) and metalorganic chemical vapour deposition are the most used methods. Each technique has certain advantages as well as disadvantages. Considering that ion implantation is a nonequilibrium process, however, it is not limited by solubility

constraints or even surface chemistry. Nevertheless, Er implantation causes large damage to the host lattice, and post-implantation annealing is necessary to improve the crystal quality of the film. This technique is a prominent technology in the semiconductor industry that allowing the introduction of doped ions in a controlled manner and with an excellent solubility in the matrix [19].

The visible PL spectra of Er ions incorporated in GaN matrix are complex owing to the existence of various emitting centers. In fact, the various defects present in the band gap of GaN host directly affect the PL emission spectra. Identification of diverse emitting centers is important to interpret the emitting properties of RE^{3+} ions and can lead to new technologies for optical devices.

To increase the performance of RE-doped GaN materials, it is significant to better understand RE ion-doped GaN semiconductors and the processes affecting the excitation of this doping ion in this host–lattice. In this paper, we present a detailed spectroscopic study of the defect centers in Er-implanted GaN thin films. The effects of Er^{3+} doping concentration and temperature on the optical properties of GaN thin films were evaluated. Er-Yb co-doped GaNwas synthesized to increase the luminescence efficiency in semiconductor thin films. The ET processes responsible for this enhancement were elucidated by a suitable energy level diagram. The temperature-sensing behavior of Er^{3+}–Yb^{3+} co-doped GaN semiconductor was investigated using the FIR technique.

2. Experimental

The GaN thin films implemented in these experiments were grown by a solid source MBE method using a Riber MBE-32 system on a p-Si (111) silicate substrate. Ga solid source was used in conjunction with a radio frequency plasma source providing atomic nitrogen. The sample was pre-treated with acetone, methanol, and deionized water before the insertion into the load-lock.

All sampleswere annealed at ~950 °C before the growth. An epilayers of ~0.8-µm thick were implanted with Er^{3+} and Er^{3+}/Yb^{3+} ions. This rare earth implantation was carried out within energy of 300 KeV, and the beam intensity was in the order of 5 $mA.cm^{-2}$. The deposited thin films were then dried in air at 150 °C for 30 min after the implantation

and annealed at 450 °C to improve their crystallinity followed by another annealing step at 1050 °C for 5 min. The surfaces of the samples were optically polished to use them for optical characterization. Two samples labelled as S1 and S2 were synthesized with $C(Er^{3+}) = 1\times10^{13}$ and $C(Er^{3+}) = 5\times10^{15}$ ions/cm^2 doping fluencies, respectively. S3 sample was co-doped (Er^{3+}/Yb^{3+}) with a similar concentration C(Er/Yb) = 1x10^{13} ions/cm^2.

PL measurements were performed by exciting the samples with a visible Ar laser line at 448 nm. The PL emission was collected and analyzed using a 1.3-m grating monochromator equipped with a microchannel plate photomultiplier tube used in the single photon counting mode. The laser beam was modulated using a SRS SR540 optical chopper. The signal was recorded using a digital storage oscilloscope controlled by a personal computer. For the low-temperature measurements from 8–200 K, a continuous flow helium cryostat was used.

3. Results and Discussions

3.1. Visible luminescence at low temperature

A direct excitation of the Er^{3+} ions below the GaN band gap (from the ground $^4I_{15/2}$ to the $^4F_{7/2}$or $^2H_{11/2}$ levels) yields a luminescence spectrum dominated by emission in the visible range extending mainly from 490–700 nm. Fig.1 shows an overview of the low temperature (8K) emission spectra of GaN at different Er^{3+} doping concentrations under excitation at 488 nm. The GaN:Er^{3+} spectra are composed of several bands, and are characteristics of intra-4f-shell transitions of Er^{3+} ions [17].

Both samples exhibit a blue-green emission band at around 505 nm. It is assigned to the radiative transition from the $^4F_{7/2}$ multiplet to the ground state $^4I_{15/2}$. A strong red emission band at 664 nm corresponds to the transition between stark sublevels from $^4F_{9/2}\rightarrow{}^4I_{15/2}$ of Er^{3+} ion. This bright red emission can be obtained by populating the $^4F_{9/2}$ level via cascade multiphonon nonradiative transitions from $^4F_{7/2}$ of Er^{3+} [7].

Also, three sharp extra lines were observed at 615, 649 and 694 nm correlate perfectly to $^5D_0\rightarrow{}^7F_{J=2,\,3,\,4}$ transitions of Eu^{3+} ions present accidently as an impurity in the reactor chamber [16]. This emission might imply an ET process between Er^{3+} and Eu^{3+} ions, which will be the subject of a future work.

The Er luminescence is overlapped with a broad emission band ranging from 510–550 nm, with a peak centered at 535 nm. This dominant band is the well-known yellow luminescent band (YL) commonly observed in the GaN system [20, 21]. Therefore, it is proposed that the usual Er^{3+} emission attributed to the $^4S_{3/2} \rightarrow {}^4I_{15/2}$ and $^2H_{11/2} \rightarrow {}^4I_{15/2}$ transitions in our sample is screened by the YL band or quenched by the presence of Eu^{3+} ions. This feature could be attributed to the ET between $^4S_{3/2}(Er^{3+})$ and $^5D_0$ (Eu^{3+}) levels whose energies are very close.Thus, it can be concluded that the presence of Eu^{3+} trace improves the red emission in favour of the green one due to the Er-Eu ET processes [22].

In GaN thin films, the YL band has been associated to native defect complexes. Hence, many defects can appear and V_{Ga}, O_N and C_N are among the most mentioned in the literature [23, 24]. Moreover, doping by implantation causes damages in the GaN lattice that are not completely removed by annealing [25]. The presence of the YL has been explained by two stage process involving i) nonradiative capture of an electron by a deep donor level and ii) a radiative recombination of this electron with a hole at a shallow acceptor [26].

Usually, YL band dominates the visible region of the PL spectrum in most of the undoped GaN samples. However, when GaN is grown by the MBE method in extremely Ga-rich conditions, the obtained samples have high resistivity due to self-compensation. Thus, other defect-related PL bands could be detected in the PL spectrum [27, 28]. To have a deeper insight of the situation, a low-temperature PL spectrum of undoped GaN sample excited with 488 nm was carried out (Fig. 2). The PL spectrum reveals the presence of a broad yellow-green band extending from 490–550 nm. A weaker shoulder located at 668 nm can be assigned to red luminescent (RL) band. The deconvolution of this spectrum reveals two peaks centered at 485 nm (GL) and 525 nm (YL) which are associated to the transitions via different charge levels of the same defect: 0/+ (GL) and -/0 (YL) [29].

It is worth noting that only in GaN grown with very low concentrations of carbon and oxygen impurities, an isolated defect, most probably the C_N dominant defect, causes the YL and GL bands [24]. Whereas, in samples grown with relatively high concentration of C and O, the C_NO_N complexes are likely to be formed and will cause the YL band but not the GL band [28]. Thus, we can explain the strong GL band in our sample by the Ga-rich conditions during MBE growth that result in the formation of relatively high

concentrations of nitrogen-vacancy. The red band appearing in GaN grown by MBE in extremely Ga-rich conditions originates from transition from a shallow donor (at a low temperature) to a deep acceptor level [30, 31]. Among possible candidates for the defect responsible for RL band, we suggest C, Si, O and V_{Ga}. Formation of complexes including these defects is also expected.

The comparison of the PL spectra of GaN:Er grown by MBE on Si (111) substrate with two different Er^{3+}concentrations shows that the emission spectra of both samples are almost identical except for their peak intensities, which are related to the Er doping concentration. It is clear that the emission intensity shows a quenching phenomenon [34]. This decrease occurs through the presence of many de-excitation pathways, which can be related to changes in the coordination or to the doped ion environment. This is an experimental evidence for the existence of ET processes. Moreover, different exchange interactions can lead to a much steeper decrease in intensity with increasing concentration [35]. Indeed, the ion–ion interactions should be considered to explain the decay profile. The observation of this effect is enhanced upon increasing the doping concentration within the host matrix [36]. Further, the transition probability by ET depends on the distance between the donor (D) and the acceptor (A) ions, R_{DA}, which decreases drastically under high doping concentration.
In case of Er^{3+} ($5x10^{15}$ ions/cm^2) concentration, the competition between the spontaneous radiative de-excitation and the ET results in an effective decrease in the emission luminescence intensity [36]. This latter has been proposed by Chen & al. to explain the trend of this quenching behavior in Er doped GaN [38].

3.2. Temperature dependence of PL emission spectra

The effect of temperature on the emission intensity of the YL band has been the topic of many reports regarding its dependence on the defect type [39]. The temperature dependent PL measurements were shown in Fig. 3, it is observed that the YL intensity decreases with increasing temperature following a different trend when compared to Er^{3+} emission.

To explain this feature, we assume that this thermal quenching behavior is determined by shallow donor ionization and thermal escape of holes from defects to the valence

band. The activation energy of this mechanism has been derived from the best fit of the temperature dependence YL intensity using the Arrhenius law (Fig.4):

$$I(T) = \frac{I_0}{1+Ce^{(E_A/KT)}} (1)$$

where I_0 is the intensity of the YL band at 0 K, C is the characteristic of the nonradiative process, E_A is the activation energy of the shallow donor. The $E_A$was obtained to be ~28 MeV corresponding to the binding energy of the O_N donor in GaN [40].

Much more interesting is the temperature dependence of the Er emission; in fact, the luminescent thermal stability is an important factor for evaluating semiconductor's performance. Moreover, the strong temperature quenching of the Er^{3+} emission intensity with decreasing band gap of the host material represents a strong drawback for Er-doped semiconductors [17]. Thus, Er-doping semiconductors with wide band gaps, like III–V nitrides seems to be a promising approach to overcome the thermal quenching of Er emission and leads to a better room temperature performance [33]. Particularly, GaN thin films doped with Er^{3+} ions have shown minimal thermal quenching of the emission intensity extending from cryogenic to elevated temperature [32].

To study the temperature influence on the emission of Er^{3+} related centers, we measured the PL of sample S1 between 8 K and 200 K. The behavior of the visible PL intensity is depicted in Fig. 3.

The spectra show identical features with a small shift of $^4F_{9/2}$ energy level position and differences in their relative band intensities. Moreover, the luminescence intensities of $^4F_{7/2} \rightarrow {}^4I_{15/2}$ and $^4F_{9/2} \rightarrow {}^4I_{15/2}$ transitions decrease about 25–30% from 8K to 60K. For higher temperatures, the intensity remains stable (see inset of Fig.3). The nonradiative decays of $^4F_{7/2}$ and $^4F_{9/2}$ levels are most probably responsible for this thermal quenching due to the high phonon energy which exceeds 700 cm^{-1}.

As the temperature increases, the YL band red shift is about ~40 MeV. This shift can be attributed to the thermal escape of electrons from deep donor level to another site with lower energy. Moreover, the YL band may exhibit red or blue shift with temperature depending on the excitation conditions [39].

A similar behavior is exhibited in the PL spectra for $^4F_{9/2} \rightarrow {}^4I_{15/2}$ transition. This red shift can be explained by the presence of potential fluctuations in GaN:Er^{3+} samples [41] or in terms of the thermal population of the higher $^4I_{15/2}$ stark sublevels [42]. Fig.5 shows the shift of the peak position to lower energy in the same temperature range. It is noticeable that the red luminescence maximum shifts following the band gap shrinkage. Indeed, it is well known that the GaN band gap reduces by 40 MeV from cryogenic temperature 10 K to 300 K. The large sensitivity of the PL peak shift to the band gap variation is typical for defects with strong electron-phonon coupling. This behavior suggests that the doped ion (defects) should involve these electronic energy levels sensitive to the band gap reduction, described by the effective mass theory.

3.3. PL emission analysis, energy level diagram and CIE study

To expand the Er^{3+}emission efficiency in the visible region and eliminate the overlap of different emission bands related to the defects in GaN, a co-doping with Yb^{3+} ions was carried out. The PL emission spectra have been recorded at 300K for Er^{3+}/ Er^{3+}–Yb^{3+} doped/co-doped GaN semiconductors in the range of 460–700 nm under the 488 nm excitation. A comparison of PL emission intensity for doped/co-doped GaN layers is displayed in Fig.6a.

These results depict the presence of a brilliant blue-green emission followed by a strong red one. The intense blue-green luminescence occurring from 472 nm to 512 nm with a maximum intensity at 490 nm is assigned to the $^4F_{7/2} \rightarrow {}^4I_{15/2}$ transition. Whereas, the second emission located at 663 nm is attributed to the $^4F_{9/2} \rightarrow {}^4I_{15/2}$ transition of Er^{3+}. Furthermore, the peaks at ~617, 647 and 685 nm in the red region of the spectra with a low intensity correspond to the electronic transitions, specifically, the $^5D_0 \rightarrow {}^7F_{J=2,\,3,\,4}$ of the Eu^{3+} ions. In this investigation, the emission band located at 488 nm appeared to be the most intense and this may be due to excitation stray light although an adequate filter was used.

The incorporation of the Yb^{3+} sensitizer in the GaN:Er^{3+} semiconductor improves the overall PL emission intensity. An intensity enhancement of about 15 times is noted for the RE emission (Er^{3+}, Eu^{3+}) in favor of the trap emission bands (GL, YL) in the co-doped sample. In fact, the Eu-Yb-Er system has already been studied in other hosts as

an efficient ET system [43]. It is well known that the Yb^{3+} ion has a high absorption cross-section leading to a large energy overlap between Er^{3+} and Yb^{3+} ions [44]. Moreover, the Yb^{3+} ion seems to reduce the emission of the defect-centers present in the host [45]. Thus, the ET process and the beneficial effect of the Yb^{3+} ions on the trap-centers emission are responsible for the enhancement of the Er^{3+} emission intensity and the quenching of the YL band in the visible region. Fig.6 exhibits also that the spectral profile displays obvious changes with co-doping by Yb^{3+} ions concerning the tint of the overall emission light. In other word, as far as the red component intensity is improved to the blue-green emission which leads to a tunable overall mixed emission intensity.

Under 488 nm wavelength excitation, Er and Yb ions are promoted to their excited levels via the ground state absorption process (GSA). As Yb^{3+} ion has a high absorption cross section, the latter process was more efficient for Yb ions and most of exciting energy was absorbed by these ions, which is transferred to Er ions through different ET mechanisms. To understanding the details of ET processes, the schematic energy level diagram is illustrated in Fig.6b.

After absorbing the 488 nm photon energy, the Yb^{3+} sensitizers are promoted to a virtual level V_1 and then the electrons in V_1 state decay nonradiatively to the $^2F_{5/2}$ excited level [46]. The excited Yb^{3+} ions, namely the donors, transfer their energy cooperatively to the neighboring activator ions (Yb^{3+}) which are transited to a second virtual level V_2 [47]. Subsequently, the acceptor ion (Yb^{3+}) relaxes radiatively to the $^2F_{7/2}$ level and releases blue emission at 493 nm corresponding to $2\ ^2F_{5/2} \rightarrow {}^2F_{7/2}$ transition.

On the other hand, the large number Er^{3+} ions are excited from the ground state ($^4I_{15/2}$) to the $^4F_{7/2}$ state via the GSA process and/or an ET (ET-1) from the virtual level V_2. The V_2 level is resonant with the $^4F_{7/2}$ level of Er^{3+} ion. Thus, these two energy states pursue the reputed law of Boltzmann distribution and the population interchange between them is quasithermal type. It is clear that two ET channels are in competition between V_2 (Yb^{3+}) level and $^4F_{7/2}$ (Er^{3+}) in both directions. However, at the same (Er^{3+}, Yb^{3+}) concentration, the V_2 (Yb^{3+}) $\rightarrow {}^4F_{7/2}$ (Er^{3+}) ET scheme dominates due to the higher Yb^{3+} absorption cross section. Therefore, the Er ions de-excite to the $^4I_{15/2}$ level and emit $^4F_{7/2} \rightarrow {}^4I_{15/2}$ blue-green emission band.

As for the red PL emission, two distinctive processes are contributing to load the population in the $^4F_{9/2}$ of Er^{3+} ion. In the first step, the Er^{3+} ion was excited to the $^4I_{11/2}$ state via the ET (ET-2) process from the excited Yb^{3+} ion. After that the nonradiative relaxation was set up and the electrons populate the $^4I_{11/2}$ emitted level. Then, these electrons were promoted to the $^4F_{9/2}$ excited level by an ET (ET-3) from Yb^{3+} ions. Finally, Er^{3+} ions were de-excited to the ground state ($^4I_{15/2}$) leading to red emission. Besides, the $^4F_{9/2}$ state can be also populated through the multiphonon relaxation process from the $^4F_{7/2}$ level of Er ions.

It is concluded that the incorporation of Yb^{3+} ions in the GaN: Er^{3+} semiconductor improves the population of the red emitting level of the Er ions. This is due to the various ET processes described above which suppress the population of the $^2H_{11/2}$/ $^4S_{3/2}$ levels leading to the disappearance of the green emission and the enhancement of the red one. Also, it is worthy to note that due to the higher lifetime of the $^4I_{13/2}$ state compared to the lifetime of the $^4I_{11/2}$ excited level, the process ET-3 is the dominant path over the ET-1 and ET-2 processes [48].

The overall emission light of the co-doped sample was evaluated using the CIE 1931 chromaticity diagram shown in Fig.7. Upon 488 nm, the color chromaticity coordinates at room temperature were found to be x = 0.301 and y = 0.396. The results show that Er^{3+}/Yb^{3+} co-doped GaN semiconductor provides a blended light with color in the white-light region. Thus, it is proposed that the studied semiconductors may be implemented for white light generation using a 488 nm laser excitation.

3.4. Temperature-sensing performance and color tunability

To study the potential of co-doped Er^{3+}–Yb^{3+}:GaN semiconductor in the realization of optical temperature sensor applications, the FIR technique was used. In this method, the fluorescence intensity emitted from two close thermally coupled states is monitored to calculate the ratio of the intensities arising from these two energy levels as a function of temperature. Certain researchers have been devoted that the FIR technique was implemented also for stark sublevels of a multiplet to monitor the temperature [49, 50].

With this inspiration, we analyzed the temperature dependent properties of the blue-green emission band corresponding to $^4F_{7/2} \rightarrow {}^4I_{15/2}$ transition of Er^{3+} ions upon 488 nm laser excitation which corresponds to the resonance absorption from the lowest stark sublevel of $^4I_{15/2}$ ground state to the $^4F_{7/2}$ level. Fig.8a exhibits the PL emission spectra occurring from 470 nm to 500 nm in the temperature range 200–300K.

Two distinct emission peaks located at 477 nm and 492 nm, respectively, have been detected. These two peaks are due to the transitions from the stark levels of the $^4F_{7/2}$multiplet to the $^4I_{15/2}$ state. It should be noted that the PL emission profile did not display any change in the peak positions with the rise in the sample temperature, while the PL emission intensity decreases gradually. This effect is generally related to the high probability of the nonradiative relaxation process between these two stark sublevels which are considered as two thermally coupled levels in quasithermal equilibrium [52]. Indeed, when the temperature increases, any possible stray light signal is constant; on the other hand, the relative population density of the $^4F_{7/2\ (i)}$ and $^4F_{7/2\ (j)}$ sublevels will change and follow the Boltzmann distribution leading to a variation in the emission intensity of these two stark components. The variation in the intensity ratio (FIR) can be expressed by the following equation [51]:

$$\mathrm{FIR} = \mathrm{R(T)} = \frac{\mathrm{I_{477}}}{\mathrm{I_{492}}} = \mathrm{A}\exp(-\Delta \mathrm{E}/\mathrm{K_B T}) = \mathrm{A}\exp(-\mathrm{B}/\mathrm{T}) \quad (2)$$

where, I_{477} and I_{492} are the PL emission intensity of the two stark components located at 477 nm and 492 nm, respectively. A is the pre-exponential parameter, B is a constant, ΔE is the energy gap between the energy stark sublevels, K_B is the Boltzmann constant and T is the sample temperature.

The variation of the intensity ratio R (T) is plotted as a function of inverse temperature in Fig.8b. It is noticeable that the R value presents an increasing tendency as the temperature rising. According to the fitting of these experimental data, the energy gap $\Delta E/K_B$ is found to be 103.38 K, whereas the estimation of the pre-experimental parameter provides a calculated value of A = 0.975. As exhibited in the insert in Fig.8b, the plot for ln (I_{477}/I_{492}) versus the inverse of temperature according to Eq. (3) verify a linear tendency which reveals the compatibility of this semiconductor in the temperature sensing applications.

Eq. (3) can be defined as follows:

$$\ln(\mathrm{FIR}) = \ln(\mathrm{A}) + (-\Delta \mathrm{E}/\mathrm{K_B T}) = \ln(\mathrm{A}) + (-\mathrm{B}/\mathrm{T})$$

where, all the terms have their usual meanings. The fitting with Eq. (3) provides $\ln(\mathrm{A}) = -0.025$ and B = 103.38K.

This behaviour is not in contrast with the relative temperature stability of the GaN:Er emission shown in Fig.3 because, in that case, the overall intensity of the luminescence emission is considered instead of the relative intensity of the various emission peaks.

These two parameters were used to estimate the sensor sensitivity S (T) which is a prominent factor for the development of optical temperature sensor applications. The rate of the change in the FIR value for two thermally coupled stark sublevels with respect to temperature result the sensitivity S (T), which is expressed as:

$$\mathrm{S(T)} = \left|\frac{\mathrm{d(FIR)}}{\mathrm{dT}}\right| = |\mathrm{FIR} \times (-\Delta \mathrm{E}/\mathrm{K_B T^2})| \quad (4)$$

Fig.9 shows the corresponding sensitivity curve, which is calculated using Eq.4. It is worthy to note that the sensitivity reaches its maximum value of 0.0015 $\mathrm{K^{-1}}$at 200K which was comparable with other sensitivities of different sensing materials doped with $\mathrm{RE^{3+}}$ ions reported in Table 1. This result suggests that the GaN:$\mathrm{Er^{3+}}$/$\mathrm{Yb^{3+}}$ possesses a good sensing ability [11, 53]. Thus, to judge the utility of this material in the realization of the display devices, it is important to analyze the color tint emanating light of this sample in the temperature range 10–300K. The color emitted from the prepared sample was examined using the Go-CIE software.

According to the results depicted in the CIE 1931 chromaticity diagram illustrated in Fig.7, the combination of the emission tone presents two modes: when the temperature increases from 10 K to 200 K, the overall emission light shifts from the blue region through the blue-green, green, yellow-greenish and finally reaching the yellow color. While at higher temperature (from 200 K up to 300 K), a reverse trend was seen. The color tint emanating light of this sample moves from the yellowish region to the cyan until it stabilizes in the white light region at room temperature. Based on these results, the developed semiconductor can be potential candidate for the production of the tunable lighting devices.

Conclusions

This work has been devoted to the optical study of Er-implanted GaN thin films using detailed optical spectroscopy in the visible region. PL measurements were performed on GaN thin films implanted with Er ions, followed by thermal annealing at a high temperature. This process favored Er^{3+} optical activation as well as promoted the appearance of the broad yellow luminescence (YL) band. We have also investigated the low-temperature (8K) emission spectra with two Er^{3+} concentrations (10^{13} and 5×10^{15} ions/cm^2) upon direct excitation with 488 nm. At the highest concentration, the quenching phenomenon was attributed to the ET process between Er and defect centers.

A temperature-dependent PL intensity study was performed on the sample containing 10^{13} ions/cm^2 in the range 8–200K. The temperature variation revealed the attenuation of emission intensity. This can be explained by i) the shallow donor ionization and ii) the nonradiative decay due to the high phonon energy. Therefore, the YL band-related defect energy activation corresponding to the binding of the O_N donor was determined.

To enhance the PL emission intensity in the visible region, a proposed GaN sample co-doped with Er^{3+}–$Yb^{3+}$was synthesized, and its luminescence characteristics were investigated under 488-nm laser excitation. The color tunability observed in the GaN:Er^{3+}/Yb^{3+} semiconductor has extended the latitude of the blue-cyan-green-yellow tunability region in the temperature range 10–300 K. At room temperature, the sample provides a blended light with color in the white-light region. The temperature-sensing performance of this material studied using the FIR technique confirmed the applicability of this phosphor material in the development of an optical temperature sensor with a high sensitivity over a wide temperature range. The maximum value of the sensitivity resulting from the FIR measurements was 15×10^{-4} K^{-1}.

References

[1] C. Rudowicz, D. Yadav, R. Kripal and P. Gnutek, Journal of Alloys and Compounds, 2016, 666, 468–475.

[2] B. Yuan, Y. Sheng, Y. Song, K. Zheng, X. Zhou, X. Xu and H. Zou, Journal of Alloys and Compounds, 2015, 644, 82–90.

[3] P. Du, L. Wang and J. S. Yu, Journal of Alloys and Compounds, 2016, 673, 426–432.

[4] H. Berthou and C. K. Jörgensen, Optics Letters, 1990, 15, 1100.

[5] M.K. Mahata, K. Kumar, V.K. Rai, Sensors and Actuators B: Chemical, 2015, 209, 775–780.

[6] M. P. Hehlen, N. J. Cockroft, T. R. Gosnell and A. J. Bruce, Physical Review B, 1997, 56, 9302–9318.

[7] A. A. Assadi, K. Damak, R. Lachheb, A. Herrmann, E. Yousef, C. Rüssel and R. Maâlej, Journal of Alloys and Compounds, 2015, 620, 129–136.

[8] Y. Chen, X. Lin, Z. Luo and Y. Huang, Optical Materials, 2004, 27, 625–633.

[9] I. Sokólska, E. Heumann, S. Kück and T. Lukasiewicz, Applied Physics B, 2000, 71, 893–896.

[10] Y. Zhao, X. Gong, Y. Lin, Z. Luo and Y. Huang, Materials Letters, 2006, 60, 418–421.

[11] B. P. Singh, A. K. Parchur, R. S. Ningthoujam, P. V. Ramakrishna, S. Singh, P. Singh, S. B. Rai and R. Maalej, Phys. Chem. Chem. Phys., 2014, 16, 22665–22676.

[12] P. G. Kik and A. Polman, MRS Bulletin, 1998, 23, 48–54.

[13] H. Ennen, Applied Physics Letters, 1983, 43, 943.

[14] S. Kim, S. J. Rhee, X. Li, J. J. Coleman and S. G. Bishop, Applied Physics Letters, 2000, 76, 2403–2405.

[15] S. Kim, S.J. Rhee, X. Li, J.J Coliman, S. Bishop, Applied Physics Letters, 2000, 76, 2403.

[16] Y. Q. Wang and A. J. Steckl, Applied Physics Letters, 2003, 82, 502.

[17] P. N. Favennec, H. L'Haridon, M. Salvi, D. Moutonnet and Y. Le Guillou, Electronics Letters, 1989, 25, 718–719.

[18] S. Coffa, A. Polman, R.N. Schwartz (Eds.), Materials Research Society Proceedings, vol. 1996, 422.

[19] C. Ronning, C. Borschel, S. Geburt and R. Niepelt, Materials Science and Engineering: R: Reports, 2010, 70, 30–43.

[20] T. Ogino and M. Aoki, Japanese Journal of Applied Physics, 1980, 19, 2395–2405.

[21] S. J. Pearton, J. C. Zolper, R. J. Shul and F. Ren, Journal of Applied Physics, 1999, 86, 1.

[22] W. S. Souza, R. O.Domingues, L. A. Bueno, E. B. da Costa, A. S. Gouveia-Neto, Journal of Luminescence, 2013, 144, 87–90.

[23] M. A. Reshchikov, physica status solidi (c), 2011, 8, 2136–2138.

[24] J. L. Lyons, A. Janotti and C. G. Van de Walle, Applied Physics Letters, 2010, 97, 152108.

[25] H. Przybylińska, A. Kozanecki, V. Glukhanyuk, W. Jantsch, D. J. As and K. Lischka, Physica B: Condensed Matter, 2001, 308-310, 34–37.
[26] D. G. Chtchekine, L. P. Fu, G. D. Gilliland, Y. Chen, S. E. Ralph, K. K. Bajaj, Y. Bu, M. C. Lin, F. T. Bacalzo and S. R. Stock, Journal of Applied Physics, 1997, 81, 2197.
[27] M. A. Reshchikov, H. Morkoç, S. S. Park and K. Y. Lee, MRS Proceedings, 2001, 693.
[28] M. A. Reshchikov, H. Morkoç, S. S. Park and K. Y. Lee, Applied Physics Letters, 2001, 78, 2882.
[29] M. A. Reshchikov and H. Morkoç, MRS Proceedings, 2004, 831.
[30] B. J. Skromme and G. L. Martinez, Mater. Res. Soc. Symp. Proc., 2000, 5S1,W9.8.
[31] D. M. Hofmann, B. K. Meyer, H. Alves, F. Leiter, W. Burkhard, N. Romanov, Y. Kim, J. Kruger and E. R. Weber, physica status solidi (a), 2000, 180, 261–265.
[32] M. Thaik, U. Hömmerich, R. N. Schwartz, R. G. Wilson and J. M. Zavada, Applied Physics Letters, 1997, 71, 2641.
[33] C. Ugolini, N. Nepal, J. Y. Lin, H. X. Jiang and J. M. Zavada, Applied Physics Letters, 2007, 90, 051110.
[34] S. Dai, C. Yu, G. Zhou, J. Zhang, G. Wang and L. Hu, Journal of Luminescence, 2006, 117, 39–45.
[35] E. Zych, Journal of Physics: Condensed Matter, 2002, 14, 5637–5650.
[36] R. E. Muenchausen, L. G. Jacobsohn, B. L. Bennett, E. A. McKigney, J. F. Smith, J. A. Valdez and D. W. Cooke, Journal of Luminescence, 2007, 126, 838–842.
[37] F. Benz, M. Yang, Y. Weng and H. P. Strunk, Journal of Luminescence, 2012, 132, 1493–1496.
[38] M. Stachowicz, A. Kozanecki, J. Y. Lin, H. X. Jiang and J. Zavada, Optical Materials, 2014, 36, 1730–1733.
[39] M. A. Reshchikov and H. Morkoç, Journal of Applied Physics, 2005, 97, 061301.
[40] W. J. Moore, J. A. Freitas, S. K. Lee, S. S. Park and J. Y. Han, Physical Review B, 2002, 65.
[41] M. A. Reshchikov, G.-C. Yi and B. W. Wessels, Physical Review B, 1999, 59, 13176–13183.
[42] M. J. V. Bell, L. A. O. Nunes and A. R. Zanatta, Journal of Applied Physics, 1999, 86, 338.
[43] R. Dey, A. Pandey, V. K. Rai, Sensors and Actuators B: Chemical, 2014, 190, 512–515.
[44] C. Strohhöfer and A. Polman, Optical Materials, 2003, 21, 705–712.
[45] A. N. Yunusova, V. V. Semashko, G. M. Safiullin, L. A. Nurtdinova, V. V. Pavlov and M. A. Marisov, Journal of Luminescence, 2014, 145, 443–447.
[46] A. K. Soni, V. K. Rai, Solid State Sciences, 2016, 58, 129–137.
[47] A. K. Soni, R. Dey and V. K. Rai, RSC Advances, 2015, 5, 34999–35009.
[48] V. Singh, V. K. Rai, I. Ledoux-Rak, L. Badie and H.-Y. Kwak, Applied Physics B, 2009, 97, 805–809.

[49] S. Zhou, S. Jiang, X. Wei, Y. Chen, C. Duan and M. Yin, Journal of Alloys and Compounds, 2014, 588, 654–657.
[50] V. K. Rai and S. B. Rai, Spectrochimica Acta Part A: Molecular and Biomolecular Spectroscopy, 2007, 68, 1406–1409.
[51] B. S. Cao, Y. Y. He, Z. Q. Feng, Y. S. Li and B. Dong, Sensors and Actuators B: Chemical, 2011, 159, 8–11.
[52] S. Tanabe, T. Ohyagi, N. Soga and T. Hanada, Physical Review B, 1992, 46, 3305–3310.
[53] S. Zhou, X. Li, X. Wei, C. Duan, M. Yin, Sensors and Actuators B: Chemical, 2016, 231, 641–645.
[54]M.K. Mahata, T. Koppe, T. Mondal, C. Brüsewitz, V.K. Rai, H. Hofsäss, U. Vetter, Phys. Chem. Chem. Phys., 2015, 17, 20741–20753.
[55]X. Cheng, K. Yang, J. Wang, L. Yang, X. Cheng, Opt. Mater., 2016, 58, 449–453.
[56]X. Wang, X. Kong, Y. Yu, Y. Sun, H. Zhang, Journal of Physical Chemistry C, 2007, 111, 15119.
[57]Ch. Li, B. Dong, Ch. Ming, M. Lei, Sensors, 2007, 7, 2652.
[58]A.S.S. de Camargo, J.F. Possatto, L.A. de, O. Nunes, E.R. Botero, E.R.M. Andreeta, D. Garcia, J.A. Eiras, Solid State Communications, 2006, 137, 1.
[59]Z.P Cai, H.Y. Xu, Sensors and Actuators A: Physical, 2003, 108, 187–192.
[60]S. K. Singh, K. Kumar and S. B. Rai, Sensors and Actuators A: Physical, 2009, 149, 16–20.

Short biography of Prof. Ramzi MAALEJ (University of Sfax-Tunisia)

Prof. Maalej is presently a full professor of Physics at the University of Sfax, Tunisia. He received MS degree in Physics from the University of Sfax in 1995 and PhD in Quantum Physics from University of Tunis El Manar in 2001 and Habilitaion HDR in 2007. He has been supervised ten PhD theses, and co-authored more than 40 peer-reviewed scientific journals. He has been invited professor in different universities in KSA, South Korea, Germany, and Portugal and given invited talks at several conferences. Currently he is leading a young research group “Photonic and Advanced Materials”. His research interests include theoretical and experimental studies of lanthanide-doped materials for emerging laser technologies, optoelectronic, temperature sensors, biosensor, and nanomedicine applications.

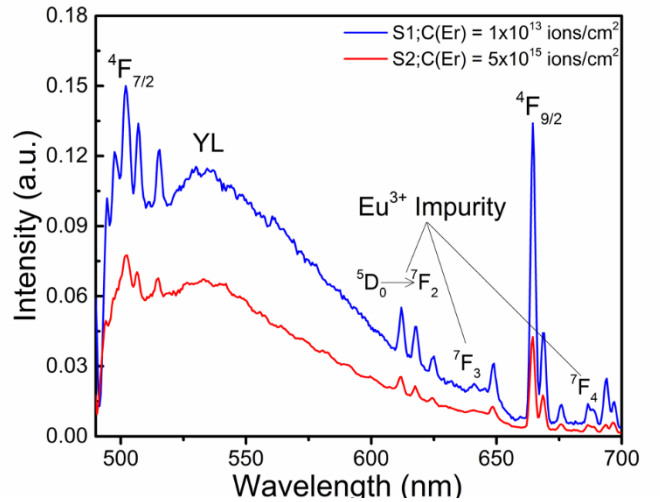

Fig.1. Emission spectra of GaN:Er^{3+} thin film at low temperature (8 K) under 488 nm excitation.

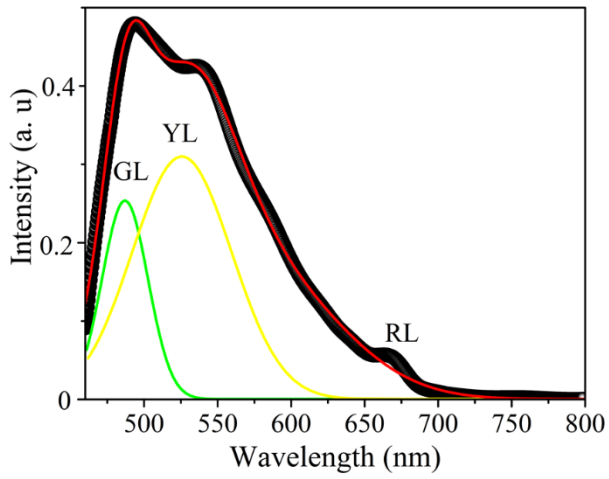

Fig.2. Emission spectrum of undoped GaN thin film at low temperature (8K) under 488 nm excitation.

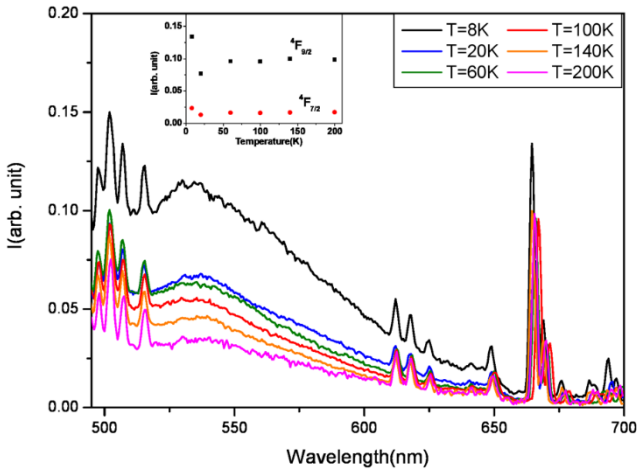

Fig.3. Emission spectra of GaN:Er^{3+} with Er^{3+} ion concentration C(Er) = $1x10^{13}$ ions/cm^2 under below-gap excitation (488 nm) over the 8–200 K temperature range. Inset shows the change in intensity of $^4F_{9/2}$ and $^4F_{7/2}$ levels with temperature (8–200 K).

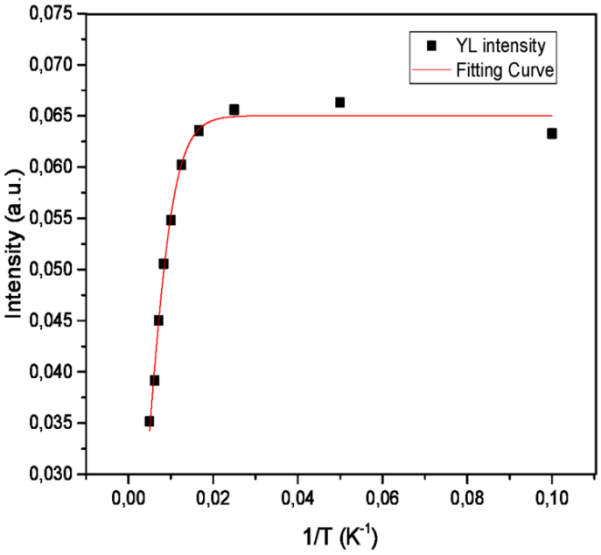

Fig.4: Temperature dependence of YL intensity band.

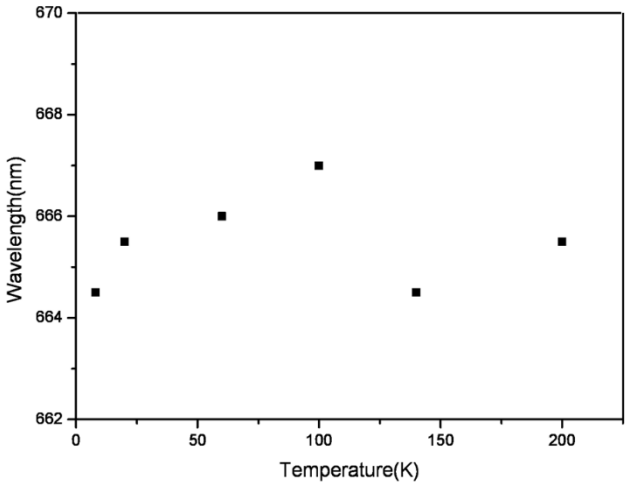

Fig.5. The change in peak position of $^4F_{9/2} \rightarrow {}^4I_{15/2}$ transition in GaN:Er film at different temperatures.

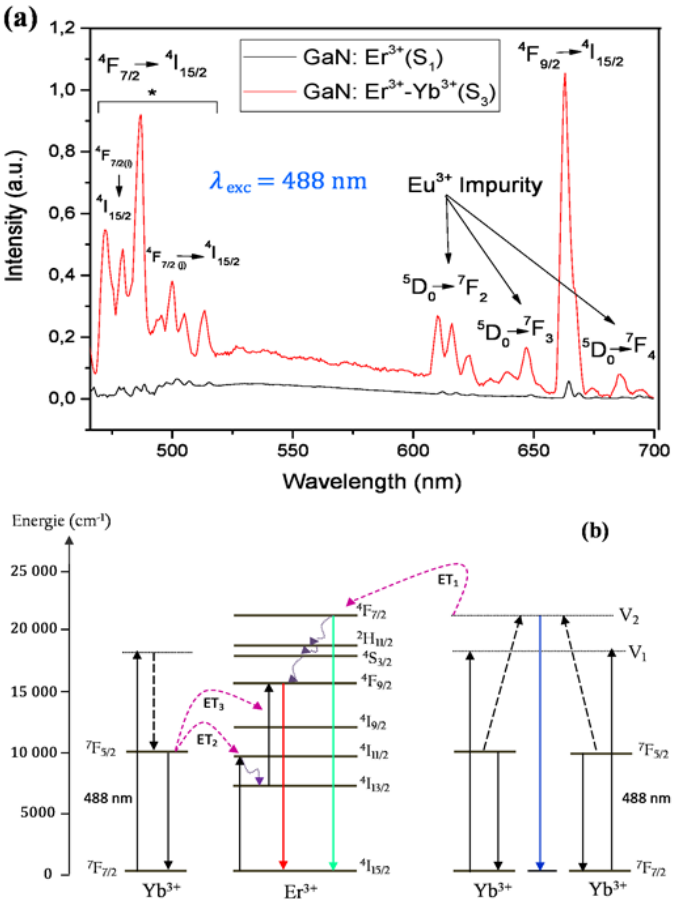

Fig.6. (a) Comparison of emission spectra for Er^{3+}/Er^{3+}–Yb^{3+} doped/co-doped GaN semiconductor at 300K under 488 nm excitation (b) Energy level diagram of Er^{3+}/Yb^{3+} system co-doped GaN semiconductor showing possible Energy Transfer at 488 nm excitation.

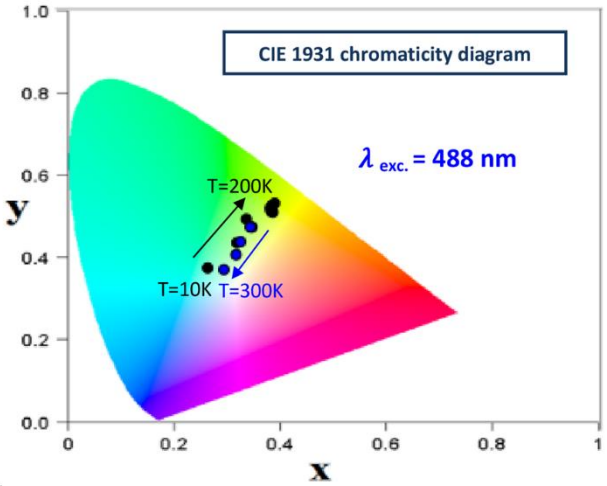

Fig.7 Color coordinate variations of co-doped GaN:Er^{3+}/Yb^{3+} in the temperature range 10-300K

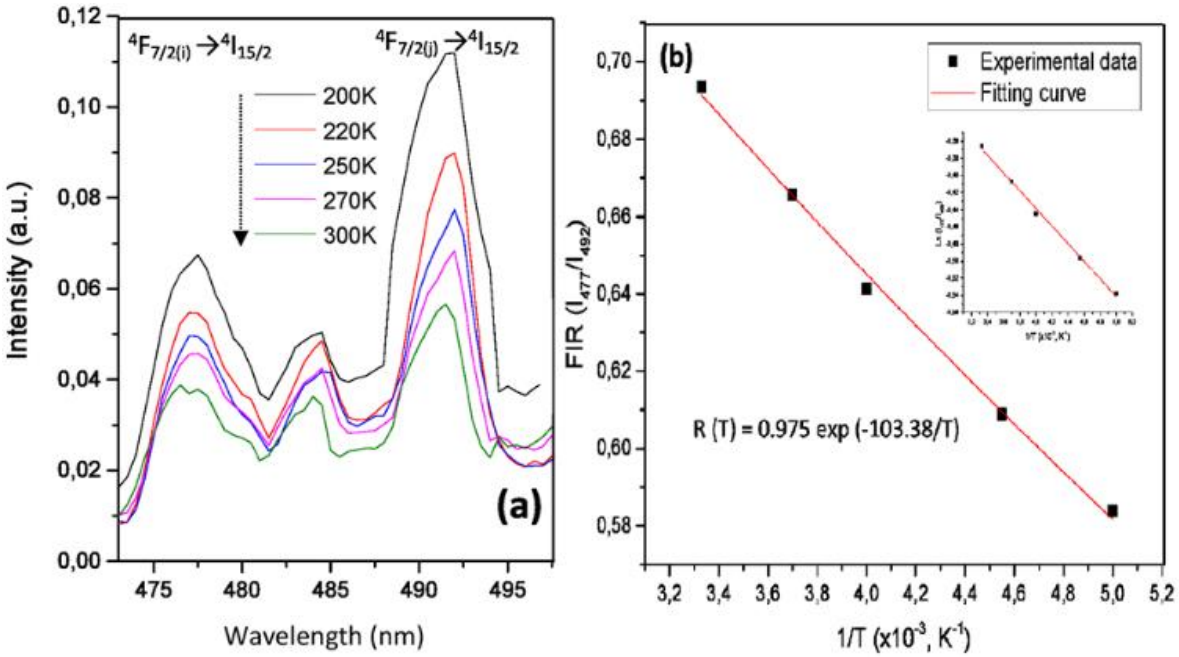

Fig.8.(a) Variation of blue-green emission bands with external temperature of GaN: Er^{3+}/Yb^{3+} thin films under 488 nm excitation. (b) Plot of FIR relative to the temperature range 200–300 K.

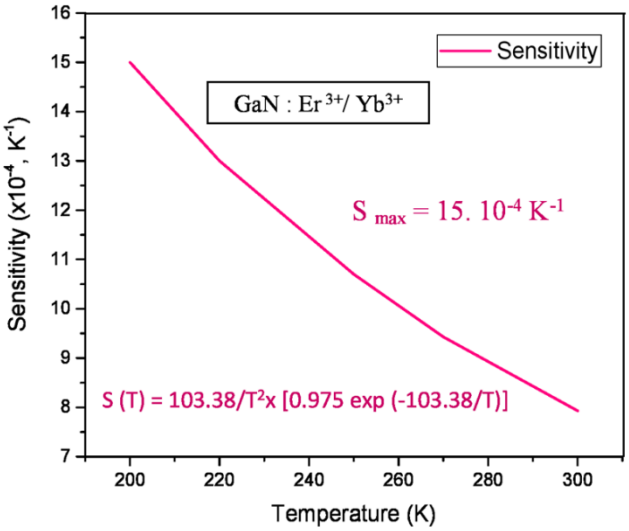

Fig.9. Sensor sensitivity as a function of temperature for GaN co-doped (Er^{3+}/Yb^{3+}) semiconductor.

Table 1. Values of the maximum sensitivity of different RE doped hosts.

RE doped samples	Maximum sensitivity ($\times 10^{-4} K^{-1}$)	T(K)	Temperature range (K)	References
ZnO:Er^{3+}	62	443	273–573	[51]
Gd_2O_3:Er^{3+}/Yb^{3+}	39	300	300–900	[55]
$CaWO_4$:Er^{3+}/Yb^{3+}	25	480	300–540	[50]
Silicate: Er^{3+}	23	296	296–673	[52]
$BaTiO_3$:Er^{3+}/Yb^{3+}	19	410	120–505	[49]
PLZT: Er^{3+}	19	556	300–610	[53]
GaN:Er^{3+}/Yb^{3+}	15	200	200–300	This work
Fluorozirconate: Er^{3+}	06	300	100–300	[54]